Elliptic flow of non-photonic electrons in Au+Au collisions at $\sqrt{s_{\rm NN}}$ = 200, 62.4 and 39 GeV

L. Adamczyk[1], J. K. Adkins[23], G. Agakishiev[21], M. M. Aggarwal[35], Z. Ahammed[53], I. Alekseev[19], J. Alford[22], C. D. Anson[32], A. Aparin[21], D. Arkhipkin[4], E. C. Aschenauer[4], G. S. Averichev[21], A. Banerjee[53], D. R. Beavis[4], R. Bellwied[49], A. Bhasin[20], A. K. Bhati[35], P. Bhattarai[48], H. Bichsel[55], J. Bielcik[13], J. Bielcikova[14], L. C. Bland[4], I. G. Bordyuzhin[19], W. Borowski[45], J. Bouchet[22], A. V. Brandin[30], S. G. Brovko[6], S. Bültmann[33], I. Bunzarov[21], T. P. Burton[4], J. Butterworth[41], H. Caines[57], M. Calderón de la Barca Sánchez[6], J. M. Campbell[32], D. Cebra[6], R. Cendejas[36], M. C. Cervantes[47], P. Chaloupka[13], Z. Chang[47], S. Chattopadhyay[53], H. F. Chen[42], J. H. Chen[44], L. Chen[9], J. Cheng[50], M. Cherney[12], A. Chikanian[57], W. Christie[4], J. Chwastowski[11], M. J. M. Codrington[48], G. Contin[26], J. G. Cramer[55], H. J. Crawford[5], X. Cui[42], S. Das[16], A. Davila Leyva[48], L. C. De Silva[12], R. R. Debbe[4], T. G. Dedovich[21], J. Deng[43], A. A. Derevschikov[37], R. Derradi de Souza[8], B. di Ruzza[4], L. Didenko[4], C. Dilks[36], F. Ding[6], P. Djawotho[47], X. Dong[26], J. L. Drachenberg[52], J. E. Draper[6], C. M. Du[25], L. E. Dunkelberger[7], J. C. Dunlop[4], L. G. Efimov[21], J. Engelage[5], K. S. Engle[51], G. Eppley[41], L. Eun[26], O. Evdokimov[10], O. Eyser[4], R. Fatemi[23], S. Fazio[4], J. Fedorisin[21], P. Filip[21], Y. Fisyak[4], C. E. Flores[6], C. A. Gagliardi[47], D. R. Gangadharan[32], D. Garand[38], F. Geurts[41], A. Gibson[52], M. Girard[54], S. Gliske[2], L. Greiner[26], D. Grosnick[52], D. S. Gunarathne[46], Y. Guo[42], A. Gupta[20], S. Gupta[20], W. Guryn[4], B. Haag[6], A. Hamed[47], L-X. Han[44], R. Haque[31], J. W. Harris[57], S. Heppelmann[36], A. Hirsch[38], G. W. Hoffmann[48], D. J. Hofman[10], S. Horvat[57], B. Huang[4], H. Z. Huang[7], X. Huang[50], P. Huck[9], T. J. Humanic[32], G. Igo[7], W. W. Jacobs[18], H. Jang[24], E. G. Judd[5], S. Kabana[45], D. Kalinkin[19], K. Kang[50], K. Kauder[10], H. W. Ke[4], D. Keane[22], A. Kechechyan[21], A. Kesich[6], Z. H. Khan[10], D. P. Kikola[54], I. Kisel[15], A. Kisiel[54], D. D. Koetke[52], T. Kollegger[15], J. Konzer[38], I. Koralt[33], L. K. Kosarzewski[54], L. Kotchenda[30], A. F. Kraishan[46], P. Kravtsov[30], K. Krueger[2], I. Kulakov[15], L. Kumar[31], R. A. Kycia[11], M. A. C. Lamont[4], J. M. Landgraf[4], K. D. Landry[7], J. Lauret[4], A. Lebedev[4], R. Lednicky[21], J. H. Lee[4], C. Li[42], W. Li[44], X. Li[38], X. Li[46], Y. Li[50], Z. M. Li[9], M. A. Lisa[32], F. Liu[9], T. Ljubicic[4], W. J. Llope[41], M. Lomnitz[22], R. S. Longacre[4], X. Luo[9], G. L. Ma[44], Y. G. Ma[44], D. P. Mahapatra[16], R. Majka[57], S. Margetis[22], C. Markert[48], H. Masui[26], H. S. Matis[26], D. McDonald[49], T. S. McShane[12], N. G. Minaev[37], S. Mioduszewski[47], B. Mohanty[31], M. M. Mondal[47], D. A. Morozov[37], M. K. Mustafa[26], B. K. Nandi[17], Md. Nasim[31], T. K. Nayak[53], J. M. Nelson[3], G. Nigmatkulov[30], L. V. Nogach[37], S. Y. Noh[24], J. Novak[29], S. B. Nurushev[37], G. Odyniec[26], A. Ogawa[4], K. Oh[39], A. Ohlson[57], V. Okorokov[30], E. W. Oldag[48], D. L. Olvitt Jr.[46], B. S. Page[18], Y. X. Pan[7], Y. Pandit[10], Y. Panebratsev[21], T. Pawlak[54], B. Pawlik[34], H. Pei[9], C. Perkins[5], P. Pile[4], M. Planinic[58], J. Pluta[54], N. Poljak[58], K. Poniatowska[54], J. Porter[26], A. M. Poskanzer[26], N. K. Pruthi[35], M. Przybycien[1], J. Putschke[56], H. Qiu[26], A. Quintero[22], S. Ramachandran[23], R. Raniwala[40], S. Raniwala[40], R. L. Ray[48], C. K. Riley[57], H. G. Ritter[26], J. B. Roberts[41], O. V. Rogachevskiy[21], J. L. Romero[6], J. F. Ross[12], A. Roy[53], L. Ruan[4], J. Rusnak[14], O. Rusnakova[13], N. R. Sahoo[47], P. K. Sahu[16], I. Sakrejda[26], S. Salur[26], J. Sandweiss[57], E. Sangaline[6], A. Sarkar[17], J. Schambach[48], R. P. Scharenberg[38], A. M. Schmah[26], W. B. Schmidke[4], N. Schmitz[28], J. Seger[12], P. Seyboth[28], N. Shah[7], E. Shahaliev[21], P. V. Shanmuganathan[22], M. Shao[42], B. Sharma[35], W. Q. Shen[44], S. S. Shi[26], Q. Y. Shou[44], E. P. Sichtermann[26], M. J. Skoby[18], D. Smirnov[4], N. Smirnov[57], D. Solanki[40], P. Sorensen[4], H. M. Spinka[2], B. Srivastava[38], T. D. S. Stanislaus[52], J. R. Stevens[27], R. Stock[15], M. Strikhanov[30], B. Stringfellow[38], M. Sumbera[14], X. Sun[26], X. M. Sun[26], Y. Sun[42], Z. Sun[25], B. Surrow[46], D. N. Svirida[19], T. J. M. Symons[26], M. A. Szelezniak[26], J. Takahashi[8], A. H. Tang[4], Z. Tang[42], T. Tarnowsky[29], J. H. Thomas[26], A. R. Timmins[49], D. Tlusty[14], M. Tokarev[21], S. Trentalange[7], R. E. Tribble[47], P. Tribedy[53], B. A. Trzeciak[13], O. D. Tsai[7], J. Turnau[34], T. Ullrich[4], D. G. Underwood[2], G. Van Buren[4], G. van Nieuwenhuizen[27], M. Vandenbroucke[46], J. A. Vanfossen, Jr.[22], R. Varma[17], G. M. S. Vasconcelos[8], A. N. Vasiliev[37], R. Vertesi[14], F. Videbæk[4], Y. P. Viyogi[53], S. Vokal[21], A. Vossen[18], M. Wada[48], F. Wang[38], G. Wang[7], H. Wang[4], J. S. Wang[25], X. L. Wang[42], Y. Wang[50], Y. Wang[10], G. Webb[4], J. C. Webb[4], G. D. Westfall[29], H. Wieman[26], S. W. Wissink[18], R. Witt[51], Y. F. Wu[9], Z. Xiao[50], W. Xie[38], K. Xin[41], H. Xu[25], J. Xu[9], N. Xu[26], Q. H. Xu[43], W. Xu [7], Y. Xu[42], Z. Xu[4], W. Yan[50], C. Yang[42], Y. Yang[25], Y. Yang[9], Z. Ye[10], P. Yepes[41], L. Yi[38], K. Yip[4], I-K. Yoo[39], N. Yu[9], H. Zbroszczyk[54], W. Zha[42], J. B. Zhang[9], J. L. Zhang[43], S. Zhang[44], X. P. Zhang[50], Y. Zhang[42], Z. P. Zhang[42], F. Zhao[7], J. Zhao[9], C. Zhong[44], X. Zhu[50], Y. H. Zhu[44], Y. Zoulkarneeva[21], M. Zyzak[15]

(STAR Collaboration)

[1] *AGH University of Science and Technology, Cracow, Poland*

[2] *Argonne National Laboratory, Argonne, Illinois 60439, USA*

arXiv:1405.6348v1 [hep-ex] 24 May 2014

[3] University of Birmingham, Birmingham, United Kingdom
[4] Brookhaven National Laboratory, Upton, New York 11973, USA
[5] University of California, Berkeley, California 94720, USA
[6] University of California, Davis, California 95616, USA
[7] University of California, Los Angeles, California 90095, USA
[8] Universidade Estadual de Campinas, Sao Paulo, Brazil
[9] Central China Normal University (HZNU), Wuhan 430079, China
[10] University of Illinois at Chicago, Chicago, Illinois 60607, USA
[11] Cracow University of Technology, Cracow, Poland
[12] Creighton University, Omaha, Nebraska 68178, USA
[13] Czech Technical University in Prague, FNSPE, Prague, 115 19, Czech Republic
[14] Nuclear Physics Institute AS CR, 250 68 Řež/Prague, Czech Republic
[15] Frankfurt Institute for Advanced Studies FIAS, Germany
[16] Institute of Physics, Bhubaneswar 751005, India
[17] Indian Institute of Technology, Mumbai, India
[18] Indiana University, Bloomington, Indiana 47408, USA
[19] Alikhanov Institute for Theoretical and Experimental Physics, Moscow, Russia
[20] University of Jammu, Jammu 180001, India
[21] Joint Institute for Nuclear Research, Dubna, 141 980, Russia
[22] Kent State University, Kent, Ohio 44242, USA
[23] University of Kentucky, Lexington, Kentucky, 40506-0055, USA
[24] Korea Institute of Science and Technology Information, Daejeon, Korea
[25] Institute of Modern Physics, Lanzhou, China
[26] Lawrence Berkeley National Laboratory, Berkeley, California 94720, USA
[27] Massachusetts Institute of Technology, Cambridge, Massachusetts 02139-4307, USA
[28] Max-Planck-Institut für Physik, Munich, Germany
[29] Michigan State University, East Lansing, Michigan 48824, USA
[30] Moscow Engineering Physics Institute, Moscow Russia
[31] National Institute of Science Education and Research, Bhubaneswar 751005, India
[32] Ohio State University, Columbus, Ohio 43210, USA
[33] Old Dominion University, Norfolk, Virginia 23529, USA
[34] Institute of Nuclear Physics PAN, Cracow, Poland
[35] Panjab University, Chandigarh 160014, India
[36] Pennsylvania State University, University Park, Pennsylvania 16802, USA
[37] Institute of High Energy Physics, Protvino, Russia
[38] Purdue University, West Lafayette, Indiana 47907, USA
[39] Pusan National University, Pusan, Republic of Korea
[40] University of Rajasthan, Jaipur 302004, India
[41] Rice University, Houston, Texas 77251, USA
[42] University of Science and Technology of China, Hefei 230026, China
[43] Shandong University, Jinan, Shandong 250100, China
[44] Shanghai Institute of Applied Physics, Shanghai 201800, China
[45] SUBATECH, Nantes, France
[46] Temple University, Philadelphia, Pennsylvania 19122, USA
[47] Texas A&M University, College Station, Texas 77843, USA
[48] University of Texas, Austin, Texas 78712, USA
[49] University of Houston, Houston, Texas 77204, USA
[50] Tsinghua University, Beijing 100084, China
[51] United States Naval Academy, Annapolis, Maryland, 21402, USA
[52] Valparaiso University, Valparaiso, Indiana 46383, USA
[53] Variable Energy Cyclotron Centre, Kolkata 700064, India
[54] Warsaw University of Technology, Warsaw, Poland
[55] University of Washington, Seattle, Washington 98195, USA
[56] Wayne State University, Detroit, Michigan 48201, USA
[57] Yale University, New Haven, Connecticut 06520, USA and
[58] University of Zagreb, Zagreb, HR-10002, Croatia

We present the measurements of elliptic flow (v_2) of non-photonic electrons (NPE) by the STAR experiment using 2- and 4-particle correlations, $v_2\{2\}$ and $v_2\{4\}$, and the event plane method in Au+Au collisions at $\sqrt{s_{\rm NN}} = 200$ GeV, and $v_2\{2\}$ at 62.4 and 39 GeV. $v_2\{2\}$ and $v_2\{4\}$ are non-zero at low and intermediate transverse momentum (p_T) at 200 GeV, and $v_2\{2\}$ is consistent with zero at low p_T at other energies . For Au+Au collisions at $p_T < 1$ GeV/c, there is a statistically significant difference between $v_2\{2\}$ at 200 GeV and $v_2\{2\}$ at the two lower beam energies.

To be submitted to Physics Letters B

INTRODUCTION

Experiments of ultrarelativistic heavy-ion collisions aim to create deconfined nuclear matter, a Quark-Gluon Plasma (QGP), and to study the QGP properties. Among the signatures of creation of a QGP is the number-of-constituent-quark scaling of elliptic flow of light and strange hadrons produced in the collisions, indicating partonic collectivity [1]. Elliptic flow is defined as the second harmonic (v_2) in the Fourier expansion of the particle azimuthal anisotropic distribution with respect to the reaction plane, $\Psi_{\rm RP}$ [2]:

$$\frac{d^2N}{dp_T d\phi} \propto 1 + \sum_{n=1}^{\infty} 2v_n(p_T)\cos(n(\phi - \Psi_{\rm RP}))\,, \qquad (1)$$

where ϕ and p_T represent the azimuthal angle and the transverse momentum of the particle, respectively. The reaction plane contains the impact parameter and the beam momenta. In practice, the estimated reaction plane is called the event plane.

Heavy quarks provide a unique probe of the QGP properties: because their masses are large compared with the thermal energy expected in heavy-ion collisions [3], they are mainly produced in interactions with high momentum transfer, very early in the heavy-ion collisions, and they are expected to interact with the QGP differently than light and strange quarks [4–6]. Moreover, the heavy quark production is sensitive to the dynamics of the nuclear medium created in the collisions [7]; measurements of their production and elliptic flow could be used to determine the fundamental properties of the QGP, such as transport coefficients (see, for instance, Ref. [8] and references therein).

Electrons from the semileptonic decays of heavy flavor mesons (also called non-photonic electrons, NPE) represent well the directions of the mother D (B) mesons, especially when electron $p_T > 1.5(3)$ GeV/c. Thus NPE v_2 serves as a proxy for heavy quark v_2.

In this paper, we present the STAR measurements of NPE v_2 using the two- and four-particle correlations [9] ($v_2\{2\}$ and $v_2\{4\}$, respectively) and the event plane method ($v_2\{\rm EP\}$) [10] in Au+Au collisions at $\sqrt{s_{\rm NN}} =$ 200 GeV at the Relativistic Heavy Ion Collider (RHIC). These approaches have different sensitivities to elliptic flow fluctuations and to particle correlations not related to $\Psi_{\rm RP}$, so called non-flow. Jets and resonance decays are considered to be the most important sources of these non-flow correlations.

In the case of $v_2\{2\}$ and $v_2\{\rm EP\}$, there are positive contributions from both v_2 fluctuations and non-flow (the event plane and two-particle correlation methods are approximately equivalent [11]). When v_2 is obtained with four-particle correlations ($v_2\{4\}$), the fluctuations give a negative contribution and the non-flow is suppressed. Therefore, $v_2\{2\}$ gives an upper limit, and $v_2\{4\}$ gives a lower limit, on elliptic flow [12].

We also present NPE $v_2\{2\}$ in Au+Au collisions at $\sqrt{s_{\rm NN}} = 62.4$ and 39 GeV. RHIC Beam Energy Scan results show that elliptic flow of inclusive charged hadrons is approximately independent of beam energy in this energy range (the difference is less than 10% for $0.5 < p_T <$ 3 GeV/c) [13]. Measurements of NPE $v_2\{2\}$ at these energies could provide information about energy dependence of the strength of heavy quarks interactions with a hot and dense nuclear medium.

DATA ANALYSIS

Three main STAR subsystems are used in this analysis: the Time Projection Chamber (TPC) [14], Barrel Electromagnetic Calorimeter (BEMC) [15] and Time-of-Flight (ToF) [16] detectors. These detectors provide tracking and particle identification. We use events with minimum-bias and high p_T (so called high tower [17]) triggers with primary vertices located within $\pm$30 cm of the TPC's geometrical center along the beam direction. We select tracks with at least 20 points measured in the TPC and at least 52% of the maximum number of possible TPC points. The distance-of-closest-approach (DCA) of a track to the collision vertex is required to be less than 1.5 cm. Collision centrality is determined using the number of reconstructed tracks in the TPC within $|\eta| < 0.5$ [18]. Events with 0-60% centrality are selected for the v_2 measurement; however, we use minimum-bias events (0-80% centrality) to increase statistics in the electron purity estimation. The data samples used in this study are summarized in Tab. I.

Electrons are identified using the ionization energy loss (dE/dx) in the TPC, the time-of-flight in the ToF detector and the energy deposited in BEMC towers. First, we select tracks with $|\eta| < 0.7$ and $0 < n\sigma_{\rm electron} < 3$, where $n\sigma_{\rm electron}$ is the number of standard deviations from the expected mean dE/dx for electrons in the TPC. The $n\sigma_{\rm electron}$ cut was chosen to optimize the purity (to reduce a potential systematic error due to hadron contamination) and the available statistics (which is crucial for the $v_2\{4\}$ measurement). For $p_T < 1$ GeV/c, the velocity β measured in the ToF is used to reject kaons: we require $|1 - 1/\beta| < 0.03$ at 200 GeV, $-0.03 < 1 - 1/\beta < 0.02$ at 62.4 GeV and $-0.03 < 1 - 1/\beta < 0.01$ at 39 GeV. Different cuts are used because of the slightly different ToF resolution at different energies. To further enhance electron identification at 39 and 62.4 GeV, we impose a more stringent requirement on $n\sigma_{\rm electron}$ ($0 < n\sigma_{\rm electron} < 2$) for these collision energies. In the p_T range where the proton dE/dx band overlaps with the electron band ($1 < p_T < 1.5$ GeV/c), we apply an additional cut

of $|1 - 1/\beta| < 0.1$ in order to reduce proton contamination. Finally, at $p_T > 1$ GeV/c, we select tracks that have a momentum-to-energy ratio in the range of $0.3 < pc/E < 2$, where E is the energy of a single BEMC tower associated with a TPC track. The BEMC has a Shower Maximum Detector (SMD), which is a proportional gas chamber with strip readout at a depth of five radiation lengths designed to measure shower shapes and positions in the $\eta - \phi$ plane, and used to discriminate between electrons and hadrons. In order to further improve the purity of the electron sample, we require tracks to occupy more than one strip in both ϕ and η SMD planes.

Collision energy	Data sample (million events)
200 GeV (minimum bias)	150
200 GeV (high tower)	41
62.4 GeV (minimum bias)	38
39 GeV (minimum bias)	81

TABLE I. Data samples used for the analysis.

Hadron contamination is estimated by first fitting a sum of Gaussian functions for charged hadrons and electrons to the $n\sigma_{\rm electron}$ distribution in narrow p_T bins. Figure 1 shows examples of such fits for the $0.7 < p_T < 0.8$ GeV/c and $3 < p_T < 6$ GeV/c bins for 62.4 GeV data. There is also a Gaussian for merged pions that arise from track merging due to the finite two-track resolution of the TPC; these have a dE/dx approximately two times larger than "regular" pions. Parameters of the Gaussian functions (mean and width) for each fit component are constrained using high purity electron and hadron samples. The parameters for electrons are fixed based on an electron sample from photon conversion in the detector material and the Dalitz decay of π^0 and η mesons. For hadrons, we use the ToF at low and intermediate p_T to select tracks with a mass close to the mass expected for that specific hadron. At high p_T ($p_T > 3$ GeV/c), pions and protons from K^0_s and Λ decays are selected, which are identified via secondary vertex reconstruction. At this high p_T range a simplified fit model (three Gaussian functions: for electrons, pions and protons combined with kaons) describes the $n\sigma_{\rm electron}$ distribution well (see Fig. 1(b)). To improve fitting in the ranges where the kaon and the proton dE/dx bands overlap with the electron band, we impose constraints on the hadron amplitudes: the amplitude of a Gaussian for a hadron there is limited by the values determined outside of that crossover range, where hadron-electron separation is feasible. These fits are then used to calculate the hadron yields within the $n\sigma_{\rm electron}$ range selected for the analysis. Purity is defined as a ratio of electrons to all tracks that passed the quality and electron identification cuts. Figure 2 (a) shows the purity as a function of p_T – the overall purity is 90% or better. Hadron contamination is only significant at 200 GeV for $p_T \sim 0.5 - 0.6$ GeV/c and $p_T \sim 0.8 - 1.1$ GeV/c due to the overlap of the kaon and the proton dE/dx bands with the electron band, and the slightly more relaxed cuts used for that data set.

The primary source of physical background for this analysis are so-called photonic electrons. These electrons originate from real photon conversion in the detector material or from Dalitz decay of light mesons (mostly π^0 and η). We identify photonic electrons using a statistical approach, as a signal in the low mass region of the di-electron m_{e+e-} mass spectrum (mass $m_{e+e-} < 0.15$ GeV/c^2) [17]. Each primary photonic electron candidate is paired with an opposite-sign electron (so-called partner) in an event. We estimate the combinatorial background in this procedure with like-sign pairs. Figure 2(b) shows an example of an m_{e+e-} distribution for minimum-bias Au+Au 62.4 GeV events. The photonic electron yield is calculated by $N_{\rm pho} = (N^{\rm UL} - N^{\rm LS})/\varepsilon_{\rm pho}$, where $N^{\rm UL}$ and $N^{\rm LS}$ are the numbers of unlike-sign and like-sign electron pairs, respectively. $\varepsilon_{\rm pho}$ is the partner finding efficiency (also called the photonic electron reconstruction efficiency) which we determine from full GEANT simulations of the STAR detector. Figure 2 (c) shows $\varepsilon_{\rm pho}$ as a function of p_T; it varies from 15% at 0.5 GeV/c to 60% at 7 GeV/c.

The "raw" non-photonic electron signal, $N_{\rm NPE}$, is given by $N_{\rm NPE} = pN_I - N_{\rm pho}$, where N_I is the inclusive electron sample and p is the purity. Besides photonic electrons, other sources of background in this analysis are weak kaon decay ($K^{\pm} \to e^{\pm}\nu\pi^0$ and $K^0_L \to e^{\pm}\nu\pi^{\mp}$), called $K_{\rm e3}$, quarkonia and other vector mesons [17]. $K_{\rm e3}$ is the largest source of that secondary background and we subtract it from our non-photonic electron sample, as described later in this section.

Figure 3 shows the non-photonic electron signal (with $K_{\rm e3}$ background subtracted) to photonic electron background ratio for Au+Au 200, 62.4 and 39 GeV. This ratio varies from 0.3 at low p_T to 1.4 at p_T above 5 GeV/c; overall, it is lower at 62.4 and 39 GeV compared to 200 GeV because the cross-section for heavy quark production decreases faster with decreasing colliding energy than does the cross-section for the photonic electron background.

To determine the non-photonic electron elliptic flow, we first measure inclusive electron v_2, photonic electron v_2 and hadron azimuthal anisotropy and their yields. Then the $v_2^{\rm NPE}$ is given by

$$v_2^{\rm NPE} = \frac{N_I v_2^I - N_{\rm pho} v_2^{\rm pho} - N_H v_2^H}{N_{\rm NPE}} \qquad (2)$$

where $N_H = (1-p)N_I$ is the hadron contamination, v_2^I the inclusive electron elliptic flow and v_2^H the hadron azimuthal anisotropy. v_2^H is calculated as the sum of v_2 for different particle species [19–21] weighted by their yields in the inclusive electron sample. These yields are estimated based on the purity studies. Elliptic flow of

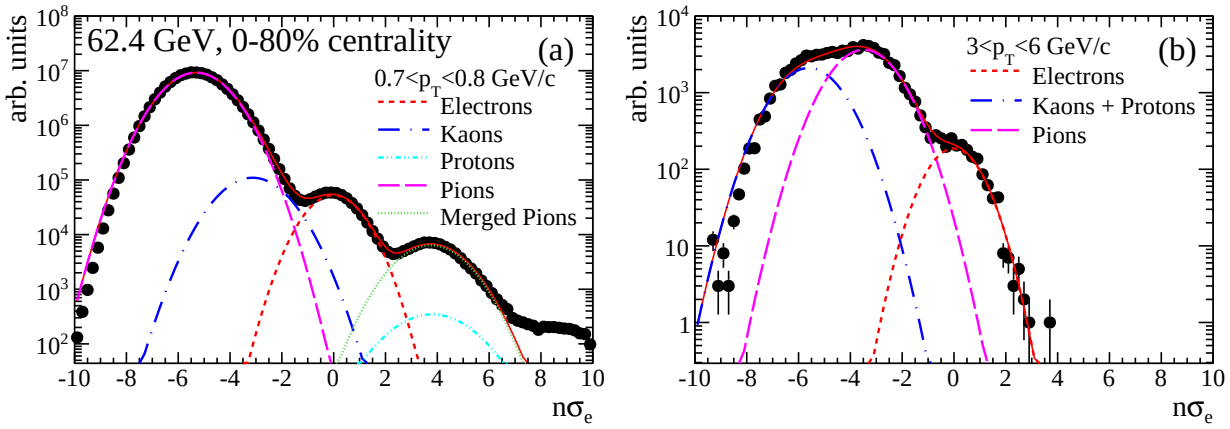

FIG. 1. (Color online) Examples of $n\sigma_e$ distribution with fits for different hadronic components for minimum bias Au+Au collisions at $\sqrt{s_{\rm NN}} = 62.4$ GeV at low (a) and high p_T (b).

these components (inclusive and photonic electrons and hadrons) can be measured using any method (for instance $v_2\{2\}$, $v_2\{4\}$ or $v_2\{\rm EP\}$).

In the $v_2\{2\}$ and $v_2\{4\}$ analyses, we obtain v_2^I and v_2^H directly from the data. Inclusive electron $v_2\{2\}$ and $v_2\{4\}$ are calculated using the direct cumulant method [22]: for $v_2\{2\}$ we correlate an electron with a single hadron, while one electron is correlated with three hadrons for $v_2\{4\}$. We calculated the reference flow using tracks with $0.2 < p_T < 2$ GeV/c within $|\eta| < 1$, excluding tracks with $|n\sigma_{\rm electron}| < 3$ to avoid self-correlations. The results are corrected for non-uniform azimuthal detector acceptance by applying the procedure described in Ref. [22]. $v_2^{\rm pho}$ is given by GEANT simulations of electrons from γ conversions and π^0 and η Dalitz decays, where the measured parent $v_2(p_T)$ and p_T spectra are required as an input. Direct photon v_2 and p_T spectra at 200 GeV are taken from Refs. [23–25]. For Au+Au 62.4 and 39 GeV, there are no published data available; therefore, we use results for $p+p$ and assume binary scaling of the direct photon yield. We use NLO pQCD calculations for $p+p$ at 62.4 GeV [26, 27] and E706 data for 39 GeV [28]. We use the $v_2(p_T)$ ($v_2\{2\}$ and $v_2\{\rm EP\}$) and p_T spectra for neutral and charged pions measured by STAR and PHENIX as input for the simulation [18, 19, 29–32], and we assume m_T scaling for η.

In the event-plane analysis, we reconstruct an event-plane using tracks with $0.15 < p_T < 1.5$ GeV/c and $|\eta| < 1$ in order to reduce the effect of jets on the event plane estimation. We exclude tracks with $|n\sigma_{\rm electron}| < 3$ to avoid possible self-correlations between the particle of interest (the electron) and tracks used in the event plane reconstruction. The results are corrected for non-uniform detector acceptance using ϕ weighting and event-by-event shifting of the planes, which is needed to make the final distribution of the event planes isotropic [10]. We obtain $v_2^{\rm NPE}\{\rm EP\}$ directly from the data: we measure the NPE production differentially at all azimuthal angles with respect to the event plane and fit the distribution with $dN/d\Delta\phi = A \times [1 + 2v_2^{\rm NPE}\{\rm EP\}\cos(2\Delta\phi)]$, where $\Delta\phi \equiv \phi - \Psi_{\rm EP}$ is the electron azimuthal angle ϕ with respect to the event plane $\Psi_{\rm EP}$, reconstructed event by event. The observed $v_2\{\rm EP\}$ coefficients are corrected for the finite event plane resolution, which is estimated from the correlation of the planes of independent sub-events [10].

The K_{e3} contribution is estimated using a full GEANT simulation of the STAR detector for both K_L^0 and charged kaons. We use the K_S^0 p_T spectra measured by STAR as an input in these simulations. The efficiency for K_{e3} reconstruction is very low at low p_T due to a DCA cut applied in the analysis: 2% at $p_T = 0.5$ GeV/c and 5% at $p_T = 1$ GeV/c. We compared the K_{e3} background to the expected heavy flavor electron yield taking into account the single electron reconstruction efficiency and acceptance. In the case of Au+Au 200 GeV, we use the NPE spectra measured by PHENIX [33] as an input. For Au+Au 39 and 62.4 GeV, the NPE p_T spectrum is not available and we use a perturbative QCD prediction for NPE production [34] scaled by the number of binary collisions. The NPE measurements in $p+p$ at $\sqrt{s_{\rm NN}} = 200$ GeV are consistent with the upper limit of the pQCD calculation; therefore, we use the upper limit on the predictions as an estimate of NPE yield at lower energies. The K_{e3} electron background is small at 200 GeV and it decreases with increasing p_T: we estimate it to be 8% for $p_T < 1$ GeV/c and less than 2% for $p_T > 3$ GeV/c. However, the heavy quark production cross-section decreases faster with decreasing energy than does the cross-section for strangeness production. Thus the relative K_{e3} electron background is larger at 39 and 62.4 GeV than at the top RHIC energy: it amounts to $\approx 30\%$ for $p_T < 0.5$ GeV/c and $\approx 10\%$ for $0.5 < p_T < 3$ GeV/c at 62.4 GeV. It is even higher at 39 GeV: $\approx 50\%$ for

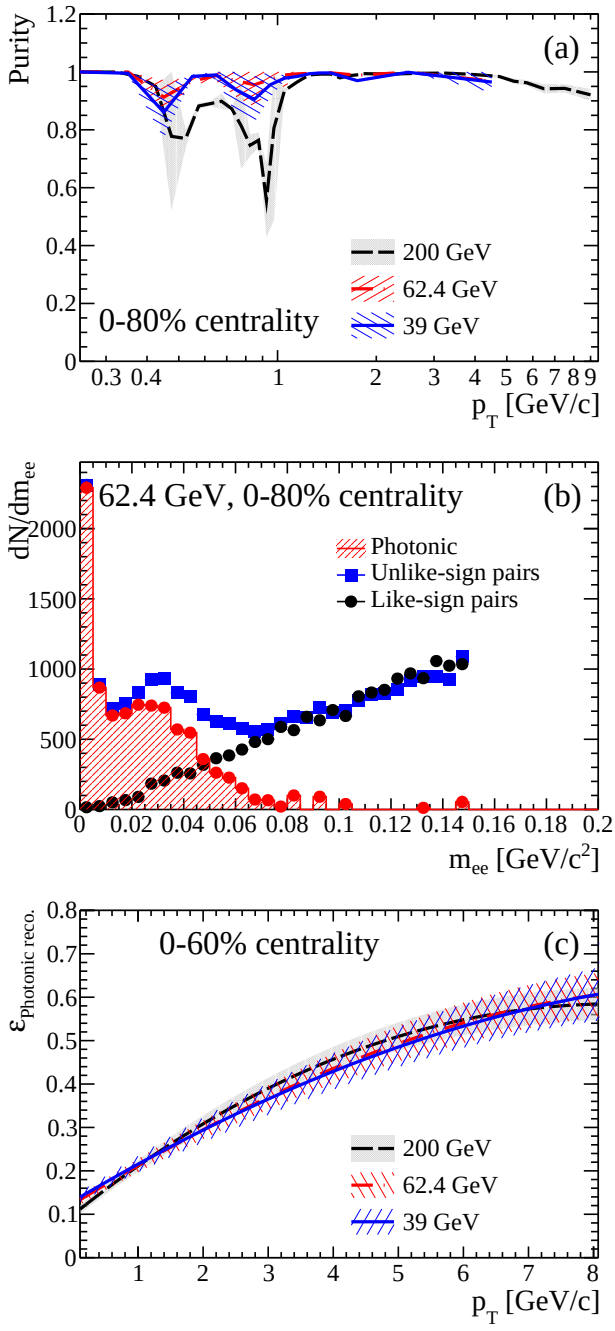

FIG. 2. (Color online) Electron purity (a), electron pair invariant mass distribution for electrons with $0.8 < p_T < 8.5$ GeV/c (b), and photonic electron reconstruction efficiency (c). The bands show combined systematic and statistical errors. Centrality classes are indicated in the plot.

$p_T < 0.5$ GeV/c and $\approx 20\%$ for $0.5 < p_T < 3$ GeV/c. We calculate the K_{e3} v_2 using a GEANT simulation of the STAR detector taking as input the kaon p_T spectrum and v_2 measured by STAR. The expected K_{e3} p_T spectrum and v_2 are then subtracted from the measured non-photonic electron yield and v_2.

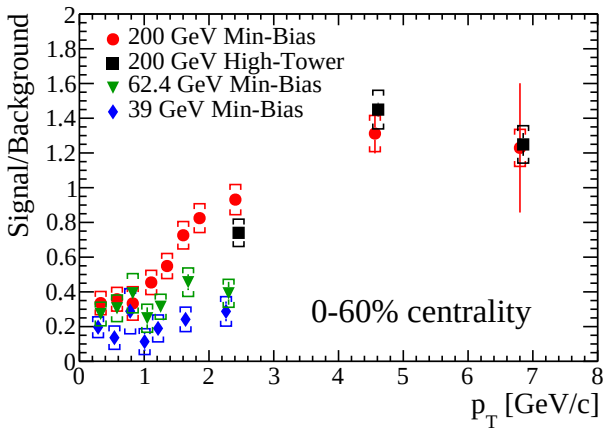

FIG. 3. (Color online) Signal-to-background ratio for non-photonic electrons at $\sqrt{s_{\rm NN}} = 200$, 62.4 and 39 GeV. The error bars represent the statistical uncertainty, and the brackets represent the systematic uncertainties. See text for details.

There are three dominant sources of systematic uncertainties in this analysis: the photonic electron reconstruction efficiency, the purity and the input parameters to the photonic electron v_2 simulation. We estimate the systematic error on $\varepsilon_{\rm pho}$ by varying the contribution of direct photons to the photonic electron yield, and by comparing the partner finding efficiency in the simulations and the data. The overall systematic error on $\varepsilon_{\rm pho}$ is $\pm 7\%$ at 200 GeV, $\pm 8\%$ at 62.4 GeV and $\pm 10\%$ at 39 GeV. The systematic error on the purity is estimated by varying the constraints in a multi-Gaussian fit. These uncertainties vary strongly with p_T; Fig. 2(a) shows the purity with the combined systematic and statistical errors. The uncertainty on the photonic electron v_2 is evaluated by varying the input spectra within their statistical and systemic errors, and varying the relative contributions of the simulation components. We estimate the systematic error on the K_{e3}/NPE ratio by varying the input NPE distribution. At 200 GeV, we vary the input spectra within statistical and systematic errors; at 39 and 62.4 GeV, we use a central value of pQCD predictions as an estimate of the lower limit on the NPE production. The overall error on photonic electron v_2 is 6% for $p_T < 5$ GeV/c; for 200 GeV at high p_T, it increases with p_T to 20% at $p_T = 7$ GeV/c.

RESULTS

Figure 4 shows the inclusive and photonic electron $v_2\{2\}$ and $v_2\{4\}$ for the 0-60% most central Au+Au collisions at 200, 62.4 and 39 GeV. The photonic electron v_2 is larger than the inclusive electron v_2 at low and intermediate p_T ($p_T < 4$ GeV/c), which indicates that the NPE v_2 has to be smaller than v_2^I. Figure 5 shows the

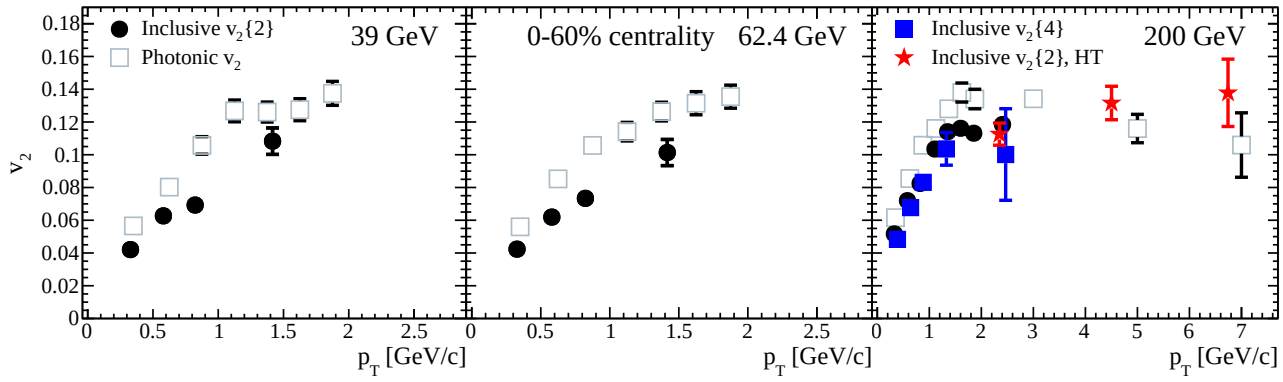

FIG. 4. (Color online) Inclusive and photonic electron $v_2\{2\}$ and $v_2\{4\}$ at $\sqrt{s_{\rm NN}}$ = 200, 62.4 and 39 GeV. The error bars represent the statistical uncertainty, and the brackets represent the systematic uncertainties. See text for details.

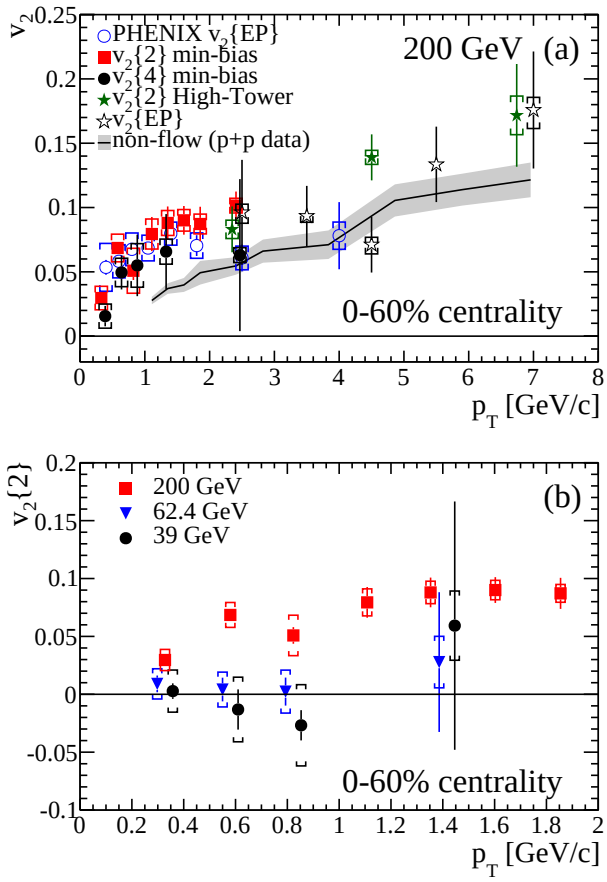

FIG. 5. (Color online)(a) Non-photonic electron azimuthal anisotropy at $\sqrt{s_{\rm NN}}$ = 200 GeV compared to PHENIX measurements [33]. (b) NPE $v_2\{2\}$ at 200 and 62.4 and 39 GeV. The error bars represent the statistical uncertainty, and the brackets represent the systematic uncertainties. Non-flow in (a) was estimated based on NPE-hadron correlations [35] for $p_T > 2.5$ GeV/c and PYTHIA for $p_T < 2.5$ GeV/c. The band includes the combined systematic and statistical uncertainties.

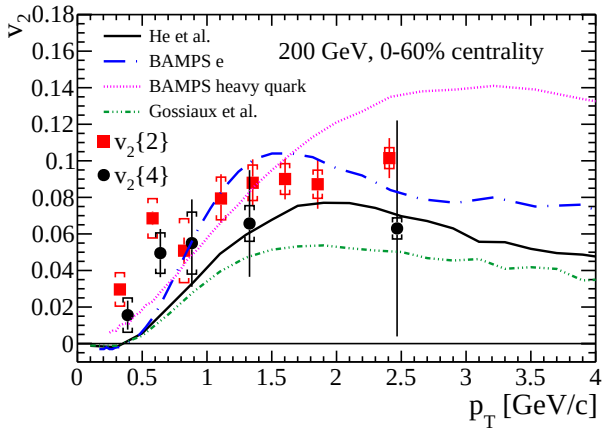

FIG. 6. (Color online) Non-photonic electron azimuthal anisotropy $v_2\{2\}$ and $v_2\{4\}$ at $\sqrt{s_{\rm NN}}$ = 200 GeV (min-bias) from Fig. 5(a) compared to model calculations.

non-photonic electron azimuthal anisotropy at $\sqrt{s_{\rm NN}}$ = 200 GeV (a), and 62.4 and 39 GeV (b). We observe finite $v_2\{2\}$ and $v_2\{4\}$ for $p_T > 0.5$ GeV/c at 200 GeV. At high p_T, the $v_2\{2\}$ and $v_2\{\rm EP\}$ results are consistent with each other, as expected. There is an increase of v_2 with p_T for $p_T > 4$ GeV/c, which is probably an effect of jet-like correlations. We estimate the strength of these correlations for $p_T > 2.5$ GeV/c using NPE–hadron correlations in $p+p$ at $\sqrt{s}$ = 200 GeV [35]; the non-flow correlations in $p+p$ are scaled by hadron multiplicity in Au+Au, similarly to Ref. [36]. If we assume that non-flow correlations in $p+p$ are similar to those in Au+Au, then the non-flow in Au+Au can be estimated by

$$v_2^{\rm non-flow} = \frac{\langle\langle 2'\rangle\rangle^{pp}}{v_2\{2\}^{\rm Ref}} \frac{\langle N_h^{pp}\rangle}{\langle N_h^{\rm AA}\rangle}, \qquad (3)$$

where $\langle\langle 2'\rangle\rangle^{pp}$ is the average two-particle correlation of NPE and hadrons in $p+p$, $\langle N_h^{pp}\rangle$ and $\langle N_h^{\rm AA}\rangle$ is the aver-

age number of hadrons in $p+p$ and Au+Au, respectively, and $v_2\{2\}^{\rm Ref}$ is the reference v_2 in Au+Au collisions. The jet-like correlation may be considerably modified in the QGP, therefore this procedure likely gives a conservative estimate of the non-flow.

We found that PYTHIA simulations, with trigger and single track reconstruction efficiency included, reproduce well the $v_2^{\rm non-flow}$ obtained with $p+p$ data at 200 GeV. Thus we use PYTHIA to estimate the $v_2^{\rm non-flow}$ for $p_T < 2.5$ GeV/c. The black solid line in Fig. 5 (a) shows the jet-like correlations expected in Au+Au collisions with the gray band representing combined statistical uncertainties and systematic uncertainties due to electron identification and photonic electron rejection [35]. Those correlations can explain the rise of $v_2\{2\}$ and $v_2\{\rm EP\}$ with p_T; more than 60% of the v_2 signal at high p_T could be explained by the central value of non-flow (black solid line). This indicates that "conventional" jet correlations (i.e. correlations unrelated to the reaction plane) are likely to dominate v_2 at $p_T > 4$ GeV/c. We did not estimate the jet-like correlation at 39 and 62.4 GeV because the NPE–hadron correlation data are not available at those energies.

STAR data are compared to the PHENIX measurements for $|\eta| < 0.35$ in Fig. 5(a). PHENIX used the beam-beam counters (BBCs) with a pseudorapidity coverage of $3.0 < |\eta| < 3.9$ to measure the event plane. A large pseudorapidity gap between the BBCs and the detector used for electron identification is expected to reduce the effect of jet-like correlations and resonance decays on the v_2 measurement. PHENIX data are consistent with STAR results in the p_T range where they overlap ($p_T \leq 4$ GeV/c).

At 39 and 62.4 GeV, $v_2\{2\}$ is consistent with zero up to $p_T = 1.6$ GeV/c (see Fig. 5(b)). We further check if the v_2 values observed for the two lower energies deviate significantly from the trend seen at top RHIC energy. We quantify the difference using χ^2 and the z-test. In the case of the z-test, $z = (\mu_1 - \mu_2)/\sqrt{\sigma_1^2 + \sigma_2^2}$, where μ is the mean and σ is the standard deviation of a given sample, $\sigma = \sqrt{\sigma_{\rm stat.}^2 + \sigma_{\rm syst.}^2}$, and the two samples are assumed to be independent of one another and to have normal distributions. The difference between results at 200 and 62.4 GeV is 1.2σ at $p_T = 0.33$ GeV/c, 3σ at $p_T = 0.58$ GeV/c and 1.7σ at $p_T = 0.82$ GeV/c, while the difference between 200 and 39 GeV is 1.2σ at $p_T = 0.33$ GeV/c, 2.3σ at $p_T = 0.58$ GeV/c and 1.8σ at $p_T = 0.82$ GeV/c. Next, we use the χ^2 test to verify the null hypothesis that $v_2\{2\}$ at 200 GeV is consistent with those at 62.4 and 39 GeV for $p_T < 1$ GeV/c. We set a significance level α at 0.01 and we define the test-statistic as

$$\chi^2 = \sum_{p_T < 1\ {\rm GeV}/c} \frac{\left(v_2^{200\ {\rm GeV}} - v_2^{\rm lower}\right)^2}{\sigma_{200\ {\rm GeV}}^2 + \sigma_{\rm lower}^2} \qquad (4)$$

where $v_2^{\rm lower}$ and $\sigma_{\rm lower}$ denote v_2 and σ for lower energies, σ is defined in the same way as for z-test and the number of degrees of freedom, NDF, is 2. The χ^2/NDF value for a consistency between 200 GeV and 62.4 GeV is 13.2/2 which corresponds to a probability $p = 0.0014$ of observing a χ^2 that exceeds the current measured χ^2 by chance, even for a correct hypothesis. For comparison between 200 and 39 GeV, χ^2/NDF = 10.5/2 which corresponds to $p = 0.005$. Thus the null hypothesis is rejected at $\alpha = 0.01$ and the difference between $v_2\{2\}$ at 200 and 62.4 GeV and 39 GeV for $p_T < 1$ GeV/c is statistically significant.

The observed v_2 for NPE is modified with respect to the parent quark v_2 due to the decay kinematics of the parent heavy hadron. This effect is shown in Fig. 6 by predictions for heavy quark elliptic flow and the resulting electron v_2 from partonic transport model BAMPS [37, 38]. Also, the NPE p_T spectrum is shifted towards lower p_T compared to the parent hadron spectra, which makes the interpretation of the NPE data model-dependent. Figure 6 shows NPE $v_2\{2\}$ and $v_2\{4\}$ at 200 GeV compared to a few models of heavy quark interactions with the partonic medium, which are described below. Note, that all models here calculate the elliptic flow of NPE and heavy quarks with respect to the reaction plane. The flow fluctuations and non-flow are not included there, therefore the predicted v_2 values should be between $v_2\{2\}$ and $v_2\{4\}$. Unfortunately, limited statistics do not allow us to quantify this difference in the data – the measured $v_2\{4\}$ is consistent with $v_2\{2\}$ within errors.

In a partonic transport model, BAMPS [37, 38] (blue dash-dotted line), heavy quarks lose energy by collisional energy loss with the rest of the medium. To account for radiative energy loss, which is not implemented in this model, the heavy quark scattering cross-section is scaled up by a phenomenological factor, K = 3.5. In BAMPS, the hadronization is implemented as fragmentation into D and B mesons using the Peterson function. Thus the observed finite v_2 of non-photonic electrons comes only from the elliptic flow of charm quarks. Indeed, heavy quarks have a large elliptic flow in this model (dotted line). Note that the Peterson fragmentation is not an appropriate description of hadronization at low p_T and other, more sophisticated mechanisms (for instance, coalescence) should be implemented. Overall, BAMPS describes $v_2\{2\}$ data well, but it slightly underestimates the nuclear modification factor $R_{\rm AA}$ for heavy flavor electrons, reported by PHENIX, at intermediate p_T ($1.5 < p_T < 4$ GeV/c) [38]. It has been shown in Ref. [39] that initial-state parton-k_T broadening (also called the Cronin effect) increases the predicted $R_{\rm AA}$ in a p_T range of 1 - 3 GeV/c and improves the agreement with the data. However, it has almost no effect at high p_T and thus it is not important for the energy loss studies.

The dash-dotted green line shows the implementation of radiative and collisional energy loss from Gossiaux et

al. [39–41]. It is a QCD-inspired model with the pQCD description of heavy quark quenching and additional non-perturbative corrections, with the hadronization implemented as coalescence at low p_T and pure fragmentation for high momentum quarks. In this model, there is little contribution from the light quark to the heavy meson v_2 and almost all the D or B meson elliptic flow comes from the charm and bottom v_2. This model describes the NPE nuclear modification factor at RHIC well, but underpredicts $v_2\{2\}$ at intermediate p_T. Nevertheless, it predicts a finite NPE v_2, which indicates a finite charm quark v_2.

The TMatrix interactions model [42, 43] is a non-perturbative approach to heavy quark energy loss. In this framework, heavy quark interaction with the medium is simulated with relativistic Fokker-Planck-Langevin dynamics for elastic scattering in a strongly coupled QGP (modeled by relativistic hydrodynamics). The model assumes strong coupling between heavy quarks and the bulk medium; hadronization is implemented by combining recombination and fragmentation. In this model, heavy quark resonances are formed in the medium at temperatures up tp 1.5 times the critical temperature T_c, and scatter off the light quarks in the QGP. The resonant rescattering increases the relaxation rates for charm quarks compared to pQCD scattering of quarks and gluons. This approach also successfully describes the nuclear modification factor, although it misses our $v_2\{2\}$ data points at intermediate p_T (solid black line). Note that v_2 should be sensitive to the heavy quark hadronization mechanism. M. He et al. [43] and P.B. Gossiaux et al. [39–41] use a coalescence approach in the shown p_T range, while in the BAMPS model heavy quarks fragment into mesons. In general, coalescence is expected to give a larger v_2 of the mesons due to the contribution of the light quark flow. However, it is shown in [33, 44] that elliptic flow of light quarks alone cannot account for the observed NPE v_2. In that model, the data are approximately reproduced if charm quarks have an elliptic flow similar to that of light quarks.

The theoretical models discussed here, despite the different mechanisms employed, assume that charm quarks are strongly coupled with the medium and have a finite elliptic flow. All these models qualitatively follow the trend of the data. To further discriminate between models, a simultaneous comparison with other experimental observables (nuclear modification factor, azimuthal correlations) as a function of beam energy is required. Our $v_2\{2\}$ measurements at 39 and 62.4 GeV provide such additional benchmarks for testing hypotheses of heavy quark energy loss. Moreover, precision measurements of these quantities for charmed and bottom hadrons separately are necessary to further constrain models and to advance our understanding of the partonic medium properties. Two new STAR detectors, the Heavy Flavor Tracker and the Muon Telescope Detector [45], will deliver such data in the next few years.

SUMMARY

We report the first measurement of non-photonic electron azimuthal anisotropy using 2- and 4- particle correlations at $\sqrt{s_{\rm NN}} = 200$ GeV, and $v_2\{2\}$ at 62.4 and 39 GeV. NPE $v_2\{2\}$ and $v_2\{4\}$ are non-zero at low and intermediate p_T at 200 GeV; more data is needed to quantify the effect of fluctuations and non-flow on the measured elliptic flow. At lower energies, the measured value of $v_2\{2\}$ is consistent with zero. The χ^2 tests for a consistency between $v_2\{2\}$ at $\sqrt{s_{\rm NN}} = 200$ GeV and lower energies for $p_T < 1$ GeV/c give $\chi^2/{\rm NDF} = 13.2/2$ for $\sqrt{s_{\rm NN}} = 62.4$ GeV, and $\chi^2/{\rm NDF} = 10.5/2$ for $\sqrt{s_{\rm NN}} = 39$ GeV. These values correspond to probabilities of $p = 0.0014$ and $p = 0.005$, respectively. Thus the difference between $v_2\{2\}$ for $p_T < 1$ GeV/c in Au+Au collisions at $\sqrt{s_{\rm NN}} = 200$ and $v_2\{2\}$ at the two lower beam energies is statistically significant.

ACKNOWLEDGEMENTS

We thank the RHIC Operations Group and RCF at BNL, the NERSC Center at LBNL, the KISTI Center in Korea and the Open Science Grid consortium for providing resources and support. This work was supported in part by the Offices of NP and HEP within the U.S. DOE Office of Science, the U.S. NSF, CNRS/IN2P3, FAPESP CNPq of Brazil, Ministry of Ed. and Sci. of the Russian Federation, NNSFC, CAS, MoST and MoE of China, the Korean Research Foundation, GA and MSMT of the Czech Republic, FIAS of Germany, DAE, DST, and CSIR of India, National Science Centre of Poland, National Research Foundation (NRF-2012004024), Ministry of Sci., Ed. and Sports of the Rep. of Croatia, and RosAtom of Russia.

[1] J. Adams, et al. (STAR Collaboration), Phys.Rev.Lett. 95 (2005) 122301.
[2] S. Voloshin, Y. Zhang, Z.Phys. C70 (1996) 665–672.
[3] R. Rapp, D. Blaschke, P. Crochet, Prog.Part.Nucl.Phys. 65 (2010) 209–266.
[4] Y. L. Dokshitzer, D. Kharzeev, Phys.Lett. B519 (2001) 199–206.
[5] N. Armesto, C. A. Salgado, U. A. Wiedemann, Phys.Rev. D69 (2004) 114003.
[6] M. Djordjevic, M. Gyulassy, R. Vogt, S. Wicks, Phys.Lett. B632 (2006) 81–86.
[7] G. D. Moore, D. Teaney, Phys.Rev. C71 (2005) 064904.
[8] S. K. Das, V. Chandra, J.-e. Alam, J.Phys. G41 (2014) 015102.
[9] N. Borghini, P. M. Dinh, J.-Y. Ollitrault, Phys.Rev. C63 (2001) 054906.
[10] A. M. Poskanzer, S. Voloshin, Phys.Rev. C58 (1998) 1671–1678.

[11] T. A. Trainor, Phys.Rev. C78 (2008) 064908.
[12] S. A. Voloshin, A. M. Poskanzer, A. Tang, G. Wang, Phys.Lett. B659 (2008) 537–541.
[13] L. Adamczyk, et al. (STAR collaboration), Phys.Rev. C86 (2012) 054908.
[14] M. Anderson, et al., Nucl. Instr. Meth. A 499 (2003) 659.
[15] M. Beddo, et al., Nucl. Instr. Meth. A 499 (2003) 725.
[16] W. Llope, Nucl. Instr. Meth. A 661, Suppl. 1 (2012) S110.
[17] H. Agakishiev, et al. (STAR Collaboration), Phys.Rev. D83 (2011) 052006.
[18] B. Abelev, et al. (STAR Collaboration), Phys.Rev. C79 (2009) 034909.
[19] J. Adams, et al. (STAR Collaboration), Phys.Rev. C72 (2005) 014904.
[20] L. Adamczyk, et al. (STAR Collaboration), Phys. Rev. C 88 (2013) 014902.
[21] L. Adamczyk, et al. (STAR Collaboration), Phys. Rev. Lett. 110 (2013) 142301.
[22] A. Bilandzic, R. Snellings, S. Voloshin, Phys. Rev. C83 (2011) 044913.
[23] A. Adare, et al. (PHENIX Collaboration), Phys.Rev.Lett. 104 (2010) 132301.
[24] S. Afanasiev, et al. (PHENIX Collaboration), Phys.Rev.Lett. 109 (2012) 152302.
[25] A. Adare, et al. (PHENIX Collaboration), Phys.Rev.Lett. 109 (2012) 122302.
[26] T. Sakaguchi (PHENIX Collaboration), Nucl.Phys. A805 (2008) 355–360.
[27] L. E. Gordon, W. Vogelsang, Phys. Rev. D 48 (1993) 3136.
[28] L. Apanasevich, et al. (Fermilab E706 Collaboration), Phys.Rev. D70 (2004) 092009.
[29] B. Abelev, et al. (STAR Collaboration), Phys.Lett. B655 (2007) 104–113.
[30] A. Adare, et al. (PHENIX Collaboration), Phys.Rev.Lett. 101 (2008) 232301.
[31] A. Adare, et al. (PHENIX Collaboration), Phys.Rev.Lett. 109 (2012) 152301.
[32] A. Adare, et al. (PHENIX Collaboration), Phys.Rev.Lett. 105 (2010) 142301.
[33] A. Adare, et al. (PHENIX Collaboration), Phys.Rev. C84 (2011) 044905.
[34] M. Cacciari, P. Nason, R. Vogt, Phys.Rev.Lett. 95 (2005) 122001. R. Vogt, private communication.
[35] M. Aggarwal, et al. (STAR Collaboration), Phys.Rev.Lett. 105 (2010) 202301.
[36] J. Adams, et al. (STAR Collaboration), Phys.Rev.Lett. 93 (2004) 252301.
[37] J. Uphoff, O. Fochler, Z. Xu, C. Greiner, Phys.Rev. C84 (2011) 024908.
[38] J. Uphoff, O. Fochler, Z. Xu, C. Greiner, Phys.Lett. B717 (2012) 430–435.
[39] P. Gossiaux, J. Aichelin, Phys.Rev. C78 (2008) 014904.
[40] P. Gossiaux, J. Aichelin, T. Gousset, V. Guiho, J.Phys. G37 (2010) 094019.
[41] J. Aichelin, P. Gossiaux, T. Gousset, Acta Phys.Polon. B43 (2012) 655–662.
[42] H. van Hees, M. Mannarelli, V. Greco, R. Rapp, Phys.Rev.Lett. 100 (2008) 192301.
[43] M. He, R. J. Fries, R. Rapp, Phys.Rev. C86 (2012) 014903.
[44] V. Greco, C. Ko, R. Rapp, Phys.Lett. B595 (2004) 202–208.
[45] H. Z. Huang (STAR Collaboration), Nucl.Phys. A904-905 (2013) 921c.